THE JOURNAL OF PHYSICAL CHEMISTRY C

Article

Cite This: J. Phys. Chem. C 2018, 122, 17211−17220

pubs.acs.org/JPCC

CO_2-Induced Displacement of Na^+ and K^+ in Zeolite |NaK|-A

Przemyslaw Rzepka,[†] Dariusz Wardecki,*[,†,‡,§] Stef Smeets,[†] Melanie Müller,[∥] Hermann Gies,[∥] Xiaodong Zou,[†] and Niklas Hedin*[,†]

[†]Department of Materials and Environmental Chemistry, Stockholm University, SE-106 91 Stockholm, Sweden

[‡]Department of Chemical and Biological Engineering, Chalmers University of Technology, SE-412 96 Göteborg, Sweden

[§]Institute of Experimental Physics, Faculty of Physics, University of Warsaw, Pasteura 5, 02-093 Warsawa, Poland

[∥]Institute of Geology, Mineralogy and Geophysics, Faculty of Geosciences, Ruhr-Universität Bochum, Universitätsstraße 150, 44780 Bochum, Germany

Supporting Information

ABSTRACT: Adsorption technologies offer opportunities to remove CO_2 from gas mixtures, and zeolite A has good properties that include a high capacity for the adsorption of CO_2. It has been argued that its abilities to separate CO_2 from N_2 in flue gas and CO_2 from CH_4 in raw biogas can be further enhanced by replacing Na^+ with K^+ in the controlling pore window apertures. In this study, several compositions of |$Na_{12-x}K_x$|-A were prepared and studied with respect to the adsorption of CO_2, N_2, and CH_4, and the detailed structural changes were induced by the adsorption of CO_2. The adsorption of CO_2 gradually decreased on an increasing content of K^+, whereas the adsorption of N_2 and CH_4 was completely nulled already at relatively small contents of K^+. Of the studied samples, |Na_9K_3|-A exhibited the highest CO_2 over N_2/CH_4 selectivities, with $\alpha(CO_2/N_2) > 21\,000$ and $\alpha(CO_2/CH_4) > 8000$. For samples with and without adsorbed CO_2, analyses of powder X-ray diffraction (PXRD) data revealed that K^+ preferred to substitute Na^+ at the eight-ring sites. The Na^+ ions at the six-ring sites were gradually replaced by K^+ on an increasing K^+ content, and these sites split into two positions on both sides of the six-ring mirror plane. It was observed that both the eight-ring and six-ring sites tailored the maximum adsorption capacity for CO_2 and possibly also the diffusion of CO_2 into the α-cavities of |$Na_{12-x}K_x$|-A. The adsorption of CH_4 and N_2 on the other hand appeared to be controlled by the K^+ ions blocking the eight-ring windows. The in situ PXRD study revealed that the positions of the extra-framework cations were displaced into the α-cavities of |$Na_{12-x}K_x$|-A on the adsorption of CO_2. For samples with a low content of K^+, the repositioning of the cations was consistent with a mutual attraction with the adsorbed CO_2 molecules.

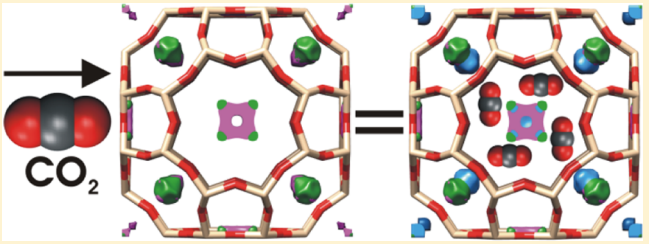

INTRODUCTION

With the combustion of fossil fuels, significant amounts of CO_2 are emitted to the atmosphere, which affects the climate and contributes to global warming.[1,2] The global energy system needs to be reformed to properly mediate the effects of climate change, and one often suggested measure is to introduce carbon capture and storage (CCS) technologies,[3] by, for example, capturing CO_2 from the flue gases of power stations. A range of postcombustion technologies can be used to capture CO_2, which includes amine scrubbers, membrane technologies, and cryogenic separation.[4] Adsorption-driven processes are expected to be more cost-effective than amine-scrubbing processes.[5−7] It is still though a bit uncertain if CCS can be economically viable[8] in the current global legal framework. In this context, note that CO_2 capture is also relevant for the upgrading of, for example, natural gas and raw biogas.[7,9−11] Upgraded biogas is arguably among the biofuels that have the lowest environmental footprint when it has been produced from appropriately selected biowaste.[12]

For the introduction of adsorption-driven CO_2 capture, it has been shown that it is important to develop highly functional and selective adsorbents for CO_2.[5,13] A high CO_2-over-N_2 selectivity can be achieved by adsorptive CO_2−N_2 partitioning on certain adsorbents in flue gas compositions typical for coal combustion (15 vol % CO_2 and 85 vol % N_2).[14,15] During adsorption, CO_2 concentrates at solid interfaces of adsorbents by chemi- or physisorption. The electronic structure of physisorbed CO_2 is not affected significantly by the adsorption, whereas during chemisorption, other species such as (bi)carbonate-like species and so on often form.[16] The most prominent mechanism of physisorption of CO_2 relates to the interactions in between the electrical field gradients (*efgs*) of the sorbent and the electric quadrupole moment of CO_2. In addition to the thermodynamically based CO_2 over N_2 selectivity of adsorbents, additional kinetic selectivity can occur because of differential diffusion rates of CO_2 and N_2. CO_2 diffuses faster than N_2 in porous solids because the CO_2 molecule has a smaller kinetic diameter than

Received: April 25, 2018
Revised: July 4, 2018
Published: July 10, 2018

DOI: 10.1021/acs.jpcc.8b03899
J. Phys. Chem. C 2018, 122, 17211−17220

N_2 in porous solids (opposite to the kinetic diameters in the gaseous state),[17,18] with typical values of 0.33, 0.36, and 0.38 nm for CO_2, N_2, and CH_4, respectively. Hence, adsorbents with effective pore openings in this range display kinetically enhanced selectivity for CO_2 and for extreme cases molecular sieving action.[19] In relation to the thermodynamics and kinetics, a wide range of adsorbent materials are studied for a potential use in the removal of CO_2 from flue gases, including zeolites, activated carbons, porous polymers, and amine-modified silica materials.[5,13,20]

Zeolites are crystalline and microporous aluminosilicates with interconnected cages and channels[21,22] and are of particular interest because of their CO_2 capacities and selectivities, robustnesses, and often low costs.[20] Zeolites with pore windows framed by eight rings (eight-membered rings, consisting of eight Si or Al atoms interconnected by O atoms) have sizes close to the effective kinetic diameters of CO_2 and N_2,[23] making them candidates for a kinetically enhanced separation of CO_2 from N_2 or CH_4.[23−31] Of particular interest is the wide variety of extra-framework cations that can be introduced into these systems to temporarily or permanently block the eight-ring windows in zeolites with low Si/Al ratios, such as in zeolite A.

Zeolite A is a synthetic eight-ring zeolite[32,33] with a Si/Al ratio close to 1 that has found many applications.[34] It consists of a primitive cubic arrangement of large cavities (referred to as α-cavities) interconnected via eight rings to form a three-dimensional channel system. |Na_{12}|-A has a high uptake of CO_2[32] and appears to be a good candidate for an adsorption-driven CO_2 capture. One should note that the Na^+ ions tailor the effective window size of eight rings in |Na_{12}|-A. The Na^+ ions block the eight-ring windows and temporarily reposition to allow adsorbates to effectively diffuse throughout its structure. |Na_{12}|-A is often assumed to have an effective pore diameter of 0.41 nm.[35,36] However, by substituting Na^+ with cations of different diameters, the size of the effective pore window apertures can be tuned.[37−39] This tunability makes it possible to further enhance the CO_2 over N_2 selectivity. |$Na_{12-x}K_x$|-A compositions with $x > 0$ have smaller pore openings than |Na_{12}|-A.[23,40] At a critical concentration of K^+ (or Cs^+), sufficiently many eight-ring windows are blocked with these ions to effectively hamper the adsorption of N_2 or CH_4.[41−43] Liu et al. showed that |$Na_{10}K_2$|-A exhibited a substantially enhanced CO_2 over N_2 selectivity but still maintained a high capacity to adsorb CO_2.[23] Earlier, Bulow et al. had shown similar findings for the separation of CO_2 and acetylene.[44] An example of the transport of CO_2, N_2, and CH_4 through |Na_{12}|-A and |Na_9K_3|-A is depicted in Figure 1, where the diffusion of N_2 and CH_4 through the 0.38 nm sized pore windows of |Na_9K_3|-A pores is hindered, but CO_2 is adsorbed in both compositions.

Narrow, or restricted, pore openings may not only enhance the kinetic selectivity of CO_2 adsorbents but will also reduce the CO_2 diffusion[37] and thus limit the corresponding mass transfer.[45−47] Such mass-transfer limitations are less ideal for adsorption-driven processes.[46−48] Akhtar et al. rationalized that |$Na_{10.8}K_{1.2}$|-A would be more suitable to adsorption-driven CO_2 capture than |$Na_{10}K_2$-A| by allowing a fast mass transfer at a high level of CO_2 over N_2 selectivity and consequently having a higher figure of merits.[49]

The crystal structures of |Na_{12}|-A and |K_{12}|-A[32,50−54] as well as the variations of different compositions of |$Na_{12-x}K_x$|-A have been carefully investigated.[23] The fine details of these structures and crystallography-related alternations during their adsorption performance are needed to better understand the CO_2 adsorption process. The overall objective of the current study was to determine the exact crystallographic positions of K^+ and Na^+ for a range of |$Na_{12-x}K_x$|-A samples and, in particular, the potential displacement of extra-framework cations on the adsorption of CO_2, as has recently been observed for the absorption of H_2O in the study of Guo et al.[55]

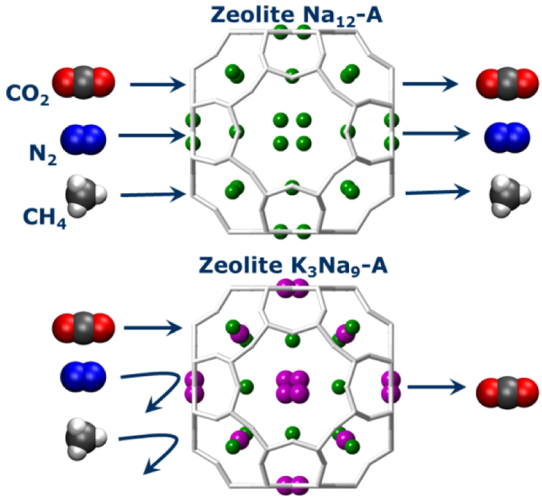

Figure 1. Overall visualization of the transport of CO_2, N_2, and CH_4 molecules through |Na_{12}|-A (top) and of only CO_2 through |Na_9K_3|-A (bottom). Na^+ sites are represented by green spheres and K^+ sites by magenta ones.

EXPERIMENTAL DETAILS

Synthesis and Experiment. The experimental work included sample preparation with K^+ exchange, elemental analysis with energy-dispersive X-ray spectroscopy (EDXS) and inductively coupled plasma optical emission spectrometry (ICP-OES), characterization of the adsorption of CO_2 (CH_4 and N_2), and investigation of crystallographic details by recording and analyzing the in situ powder X-ray diffraction (PXRD) data with and without CO_2 being adsorbed. The powder of |Na_{12}|-A was purchased from Luoyang Jianlong Chem. Ind. Co. (product number: e0002), and the batch contained relatively homogeneous cubic particles with an average size of about 2.7 μm. The quality of the batch was carefully investigated by scanning electron microscopy−EDXS and ICP-OES, and no meaningful impurities were detected. The Si/Al ratio was ∼1:1. The |$Na_{12-x}K_x$|-A samples were prepared from |Na_{12}-A| by ion exchange (Table S1) using a modified version of the procedure of Liu et al.[23]

The elemental compositions (levels of ion exchange) were evaluated by EDXS using a JEOL JSM-7000F scanning electron microscope. Thin layers of zeolite powders were spread on ink-coated aluminum stumps. The EDXS spectra were acquired under 15 keV. The elemental analyses were confirmed by ICP-OES using a PerkinElmer spectrometer model Plasm 40.

The adsorption and desorption isotherms of CO_2, CH_4, and N_2 were recorded on a Micromeritics ASAP 2020 surface area and porosity analyzer with a vacuum−ambient pressure regime capacity. Before experimentation, the zeolite samples were degassed. The samples were evacuated under high dynamic

DOI: 10.1021/acs.jpcc.8b03899
J. Phys. Chem. C 2018, 122, 17211−17220

vacuum (1 μTorr), provided by a turbopump, at a temperature of 623 K for 10 h. The temperature was ramped to the set point with a rate of 10 K/min. Thereafter, the samples were backfilled to an ambient pressure of dry N_2 at a temperature of 323 K. The dry and backfilled samples were weighed. For the gas adsorption experiments, the quasi-equilibrium states were established by waiting until the changes of pressure became <0.01% during an interval time of 15 s. The tube-free spaces for the samples were evaluated by the loading of He gas. It was assumed that He was not adsorbed.[56] The data for adsorption and desorption of CO_2, CH_4, and N_2 were collected at a temperature of 273 K set by an ice bath. The low-pressure incremental dosing mode with a dose amount of CO_2 of 0.2 mmol/g was used to achieve a good resolution of the adsorption isotherm at low pressures of CO_2. The desorption branch was terminated at 20 kPa because of the experimental constraints (the ice bath size, number of points, and equilibration time).

PXRD measurements were performed with the use of the synchrotron radiation on beamline P02.1 at PETRA III in Hamburg, Germany. Eight different samples of $|Na_xK_{12-x}|$-A were studied using a custom-made in situ gas cell at a wavelength of 0.20702(1) Å. The powdered samples were placed in borosilicate glass capillaries with a diameter of 0.7 mm and assembled to the gas cell connected through a valve either to a vacuum pump or to a gas rig with CO_2. For each sample, the following sequence of measurements was performed: (i) 5 min of data acquisition for the as-prepared samples at room temperature, (ii) dehydration of the sample for 40 min at a temperature of 573 K under dynamic vacuum conditions and then 5 min of data acquisition under the same conditions, and (iii) insertion of CO_2 at a pressure of 105 kPa and cooling down to a temperature of 273 K and then data acquisition at a low temperature for 5 min. The diffraction data were collected using a 2D PerkinElmer XRD 1621 detector, which were subsequently integrated using the FIT2D[57] program to obtain one-dimensional powder diffraction patterns with steps of 0.001° in the 2θ range of 0.5−17.5 (°). The Rietveld analyses were performed using the program Topas[58] using only the data from the activated samples and those with adsorbed CO_2.

The crystal structure of zeolite A is typically described in the space group $Fm\bar{3}c$ ($a \approx 24.6$ Å). Although the structure refinements converged in this space group, we decided to use $Pm\bar{3}m$ ($a \approx 12.3$ Å) in further analyses. This choice did not consider the SilAl ordering of the framework[50,51] (which was beyond the scope of our work), and therefore, the number of parameters could be reduced, which stabilized the refinement. Moreover, the reflections associated with the superstructure, such as (5 3 1), were within the background noise. Hence, the lattice parameter of $a \approx 12.290$ Å was derived.

All diffraction patterns were treated in a similar manner, and the atomic form factors for the framework ions for Si^{2+}, $Al^{1.5+}$, and O^- were used in analogy with the work of Pluth and Smith.[50,51] The initial sets of structure parameters for the boundary compositions $|Na_{12}|$-A and $|K_{12}|$-A were also adopted from the studies of Pluth and Smith.[50,51] The background of the diffraction data was modeled using the 23rd order Chebyshev polynomial, and the peak shapes were described by a pseudo-Voigt function (fundamental approach[59]). The total number of free parameters varied from 46 to 55 depending on the compositions and if CO_2 molecules were present. In order to stabilize the refinements, some of the isotropic thermal parameters were fixed. Moreover, because of their high correlation with other parameters, occupancies of the cations at some positions were also restrained and parameterized in accordance with the elemental analysis. Fourier difference maps were computed with a model containing only the framework atoms. These difference maps revealed several distinct features in the electron densities, which were recognized as possible cations and/or CO_2 molecules (Figures S27−S34), and several positions of peaks in the maps were used as input parameters in the Rietveld refinements. These refinements resulted in the final crystal structures with and without CO_2 adsorbed.

RESULTS AND DISCUSSION

Adsorption of CO_2, N_2, and CH_4 on $|Na_{12-x}K_x|$-A. The adsorption and crystallographic studies were conducted on a range of $|Na_{12-x}K_x|$-A samples with elemental compositions presented in Table 1 (the ICP-OES data were used in further analyses as ICP was judged to be the most precise method). $|Na_9K_3|$-A had the composition closest to those observed to have very high CO_2 over N_2/CH_4 selectivities in other studies.[23,40]

Table 1. Elemental Analysis of As-Prepared Samples Provided by EDXS and ICP-OES in Comparison to Rietveld Analyses of PXRD Data

EDXS	ICP-OES	PXRD Rietveld refinements
$\|Na_{12}\|$	$\|Na_{12}\|$	$\|Na_{12}(H_2O)_{3.0}\|$
$\|Na_{9.4}K_{2.6}\|$	$\|Na_9K_3\|$	$\|Na_{8.7}K_{3.5}(H_2O)_{0.5}\|$
$\|Na_{5.9}K_{6.1}\|$	$\|Na_6K_6\|$	$\|Na_{5.7}K_{6.3}(H_2O)_{0.6}\|$
$\|Na_{5.1}K_{6.9}\|$	$\|Na_{5.3}K_{6.7}\|$	$\|Na_{5.1}K_{7.0}(H_2O)_{0.6}\|$
$\|Na_{3.5}K_{8.5}\|$	$\|Na_{3.8}K_{8.2}\|$	$\|Na_{3.5}K_{8.5}(H_2O)_{0.6}\|$
$\|Na_{1.5}K_{10.5}\|$	$\|Na_{1.4}K_{10.6}\|$	$\|Na_{1.3}K_{10.8}(H_2O)_{1.0}\|$
$\|Na_{0.2}K_{11.8}\|$	$\|Na_{0.2}K_{11.8}\|$	$\|K_{12.2}(H_2O)_{0.7}\|$

The CO_2 adsorption and desorption isotherms for $|Na_{12-x}K_x|$-A are presented in Figure 2a, and similar families of isotherms have been reported by Liu et al. and Cheung et al.[23,40] However, in contrast to Liu et al.,[23] we did not observe any pressure-induced CO_2 uptake for the samples with high K^+ content. It is noteworthy that the CO_2 desorption and adsorption isotherms differed at low pressures of CO_2, especially for the K^+-rich samples. This increasing discrepancy between the adsorption and desorption branches can be related to the contributions of chemisorption of CO_2,[60,61] but it could also relate to loading-dependent diffusion of CO_2, or the fraction of entrapped CO_2.[62] The differentiation of physisorbed and chemisorbed CO_2 with adsorption tools is difficult. However, it is well established by infrared studies that a fraction of the CO_2 chemisorbs/reacts and (bi)carbonates are formed on zeolite $|Na_{12-x}K_x|$-A.[60,63]

At pressures of 15 and 105 kPa, the adsorption of CO_2 declined gently, almost linearly, with the content of K^+ (Figure 2b). It is observed that the K^+ ions, substituting Na^+ in the pore window apertures (the eight rings), had restricted the effective pore volume of the adsorbent and introduced a free-energy barrier to the diffusion of CO_2 among the interconnected α-cavities. In contrast to this study, Liu et al.[23] observed three stages of dependency between the adsorption of CO_2 and the K^+ content. The difference between these studies could relate to the diffusion of CO_2. We used an extended equilibration time in this study. Potentially, it could

DOI: 10.1021/acs.jpcc.8b03899
J. Phys. Chem. C 2018, 122, 17211−17220

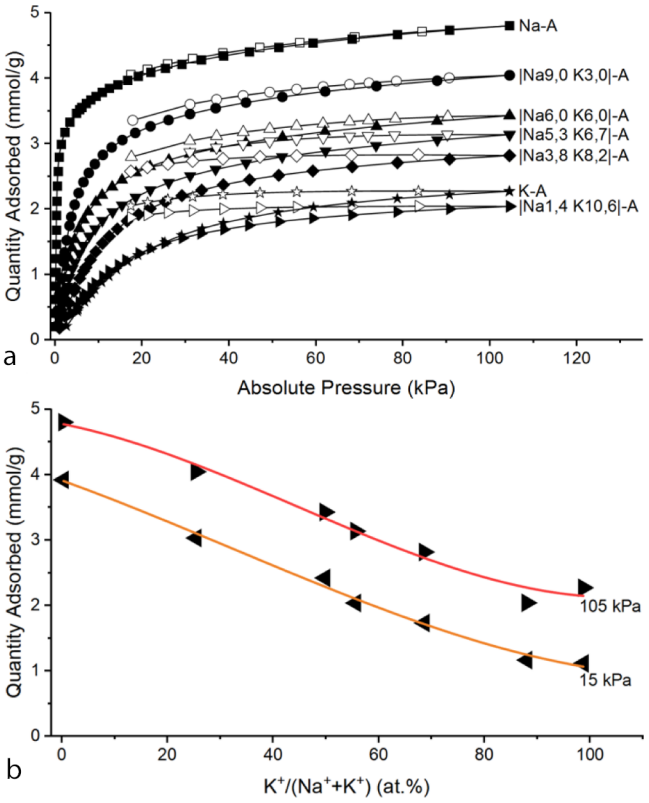

Figure 2. (a) Adsorption (solid markers) and desorption (open markers) isotherms for CO_2 on $|Na_{12-x}K_x|$-A with different K^+ contents (273 K). (b) Adsorption of CO_2 at 15 kPa and at 105 kPa as a function of K^+ content in zeolite A (%); the lines are guides for the eye.

also have been related to the type of sample or sample preparation; Liu et al. activated another type of commercial zeolite A in a flow of hot N_2[23] instead of the dynamic vacuum equilibration used here. Note that the CO_2 uptake curves depend on the equilibration time used for recording the adsorption and desorption branches on samples with a high K^+ content, and we used as long times as was judged experimentally feasible (4 days of experimental time). Still there are minor contributions from kinetics in the data.

The adsorption of CO_2 on $|Na_{12-x}K_x|$-A includes physisorption[60,61] and chemisorption as (bi)carbonate groups.[55,64,65] CO_2 is expected to physisorb on three different cation sites at low and intermediate loading levels, and at high loadings, it fills the pores (the precise location of chemisorbed CO_2 has been less well studied). Hence, CO_2 cannot be described adequately by simple adsorption models, such as the single-site Langmuir model.[66] The dual-site Langmuir (DSL) model is more suitable and commonly used.[66] We parameterized the CO_2 adsorption isotherms for $|Na_{12}|$-A and $|Na_9K_3|$-A in such a DSL model by minimizing the composite sum square deviation with a Levenberg–Marquardt iteration algorithm. The corresponding parameters are presented in the Supporting Information (Table S1). It is noteworthy that the adsorptive uptake capacity for CO_2 (q_{sat1} and q_{sat1}) was relatively similar for $|Na_{12}|$-A and $|Na_9K_3|$-A, whereas the constants b_{1+2} were significantly larger for $|Na_{12}|$-A. Despite the cross-correlation among the parameters in the DSL model,[67] this finding is consistent with the fact that the adsorption of CO_2 was kinetically slightly hampered for $|Na_9K_3|$-A at a low pressure of CO_2 and that the CO_2 diffusion was loading-dependent.

The adsorption of N_2 and CH_4, shown in Figure 3, was significantly reduced for $|Na_9K_3|$-A as compared with that for

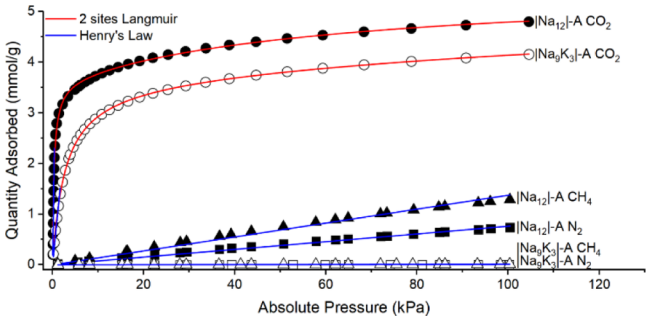

Figure 3. Adsorption isotherms for CO_2, N_2, and CH_4 on $|Na_{12}|$-A and $|Na_9K_3|$-A recorded at 273 K. The regression lines for the adsorption of CO_2 were derived with respect to the experimental data using a two-site Langmuir isotherm model and with a linear Henry's law model for the CH_4 and N_2 uptake.

$|Na_{12}|$-A, and Henry's isotherm conforms to the experimental data. Such isotherms are linearly dependent on the pressure,[68] and in the registered regime, intermolecular interactions are limited.[69] Also, the very low pressure regime for the adsorption of CO_2 could be analyzed in Henry's law model. Henry's constants of N_2 and CH_4 were 100–200 times smaller for $|Na_9K_3|$-A than for $|Na_{12}|$-A (Table S3). It is noted that the K^+ ions had effectively obstructed the adsorption of N_2 and CH_4. In the very low pressure regime, CO_2 over N_2/CH_4 selectivities can be described with the ratio of Henry's constants.[70] Within this description, $\alpha[CO_2/N_2(CH_4)]$ was 780(430) for $|Na_{12}|$-A and 22000(8300) for $|Na_9K_3|$-A. The applicability of these very low pressure selectivities is certainly limited,[66] and competitive adsorption could sometimes further enhance the selectivity.[71,72] As is well established for zeolites with low Si/Al ratio, the *efgs* are quite high,[73] and the absolute value of the quadrupolar moment is much higher for CO_2 than for N_2 (quadrupole moment of CO_2 $Q = (-14.27 \pm 0.61) \times 10^{-40}$ cm^2)[74]). CH_4 lacks a quadrupole moment. Hence, the CO_2 molecules tend to be adsorbed to the cations at much lower pressure than N_2 or CH_4 at the same temperature, and the obtained selectivity parameters are most likely to be considered as being conservative.

Structure Refinement of $|Na_{12-x}K_x|$-A with Adsorbed CO_2. The PXRD experiments and analyses were performed to give insights into the mechanism of the adsorption of CO_2 on $|Na_{12-x}K_x|$-A. The structural analyses allowed investigating changes of the positions of cations in $|Na_{12-x}K_x|$-A on the adsorption of CO_2. The Bragg peak intensities in the PXRD patterns varied significantly before and after the adsorption of CO_2. For example, the reflection intensity at $2\Theta = 1°$ was reduced on CO_2 adsorption (Figures S20–S26), indicating that the cations had been displaced.

To further analyze the effects of the adsorption of CO_2 on the structures of zeolites, the PXRD data of activated $|Na_{12-x}K_x|$-A compositions were analyzed (Tables S5–S11) and refined prior to the detailed analyses of the PXRD data recorded after the adsorption of CO_2 (Tables S20–S26). Figure 4 displays the large α-cavity and one β-cage (sod unit) in the unit cell of zeolite A, including the cation positions. The α-cavities are connected via eight-ring windows that allow

DOI: 10.1021/acs.jpcc.8b03899
J. Phys. Chem. C 2018, 122, 17211–17220

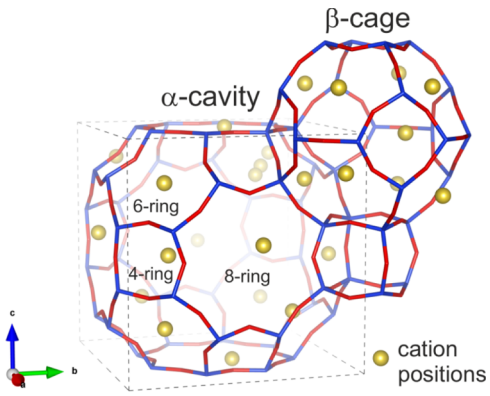

Figure 4. Overall visualization of the distribution of cation positions in α-cavities and β-cages in $|Na_{12-x}K_x|$-A. Note that K^+ occupies different positions on four- and six-ring sites than Na^+. The dashed line outlines the unit cell.

diffusion of small gas molecules (Figure 4). The α-cavities and β-cages are joined by six rings (Figure 4). As has been mentioned, the framework of $|Na_{12-x}K_x|$-A has a Si/Al ratio of ~1:1. For zeolite A, described in space group $Pm\bar{3}m$, the 12 monovalent cations per unit cell are situated at specific positions at the four-ring, six-ring, and eight-ring sites of the α-cavity. In $|Na_{12}|$-A, eight Na^+ are positioned in the center of the six rings (at different Wyckoff positions) denoted by 8g, three Na^+ are positioned close to the center of the eight rings and denoted by 12i, and a single Na^+ is positioned near the four rings and denoted by 12j. The cation distribution of $|K_{12}|$-A differs from that of $|Na_{12}|$-A because the large K^+ ions do not fit in the same positions.[51] Hence, the eight-ring site retains the same position (12i) for K^+, whereas the 8g position splits into two locations on both sides of the six rings.[51,52] Likewise, K^+ in the four rings sits in two positions: one at 12j, the same as for Na^+, and a new position at 6e. The double positioning at the four and six rings means that the K^+ cations also occur within the β-cages.

The structures for the activated $|Na_{12-x}K_x|$-A compositions, with $12 > x > 0$, appeared to be portrayed by combinations of the $|Na_{12}|$- and $|K_{12}|$-A models. Figure 5 outlines the Na^+ and K^+ populations of each site as derived from the analyses of the recorded PXRD data. The small Na^+ tends to be situated more off-center of the eight rings than the larger K^+, although both are still located in the mirror plane of the eight rings in contrast

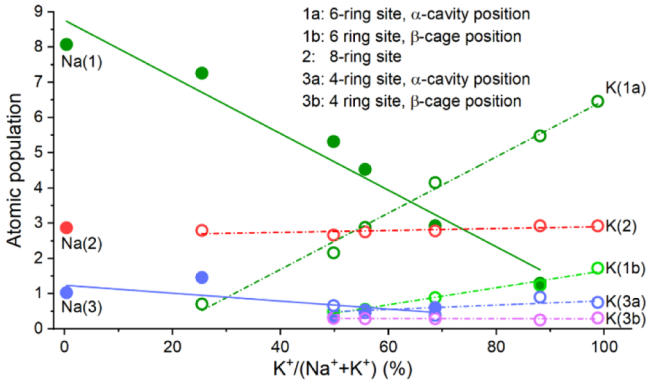

Figure 5. Population of Na^+ and K^+ at different sites in $|Na_{12-x}K_x|$-A as a function of K^+ content (%). Solid and dotted lines are "guides for the eyes" for respective Na^+ and K^+ populations.

to the cases for even larger cations.[42,54] Hence, the comparison of the electron densities in the Fourier difference maps computed for $|Na_{12}|$-A and $|Na_{12-x}K_x|$-A (Figures S27–S30) revealed that Na^+ at the eight-ring site had been already fully replaced by K^+ for the $|Na_9K_3|$-A sample (Figure 6). This

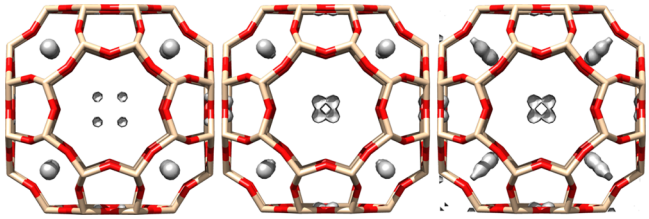

Figure 6. Difference Fourier maps for activated $|Na_{12}|$-A (left), $|Na_9K_3|$-A (middle), and $|Na_{5.3}K_{6.7}|$-A (right) computed from the experimental PXRD data with a model containing only the framework atoms.

finding is in agreement with the results from Liu et al.[23] who stated that K^+ preferred the eight-ring sites at the low content of K^+. As Na^+ preferred to sit in the six-ring mirror plane, and K^+ was off-plane, their positions and occupancies could be distinguished easily by using Fourier difference maps (Figure 6). K^+ was found to gradually substitute Na^+ at the six-ring sites on an increasing K^+ content (Figure 5) and was placed on both sides of the six rings (Figures 6, S6–S10, and S27–S29). K^+ on the four and six rings had occupancies also inside the β-cages in the K^+-rich compositions (Figures 6, S6–S10, and S27–S29). The occupied positions are denoted as 6e and 8g, respectively. K^+ positioned in the β-cage has been reported before by Leung et al.[52] and Pluth and Smith.[51]

Diffraction patterns for $|Na_{12}|$-A with and without adsorbed CO_2 are presented in Figure 7 together with a Fourier map that illustrates how the extra-framework electron densities change on the adsorption of CO_2 (Figure 7c). The diffraction data recorded before and after adsorption of CO_2 on $|Na_{12}|$-A were highly consistent with the models having final R-values of $R_{wp} \approx 1.597$, 1.564% and $R_{exp} \approx 1.074$, 1.089% (Table S4). The relative Bragg peak intensities were significantly different in the data for $|Na_{12}|$-A without CO_2 (Figure 7a) and with CO_2 adsorbed (Figure 7b). The intensity difference was related to adsorbed CO_2 and displaced Na^+. The data were processed by using the locations of the adsorbed CO_2 molecules as observed in the corresponding Fourier difference maps (Figures S31–S34). The CO_2 molecules were modeled as rigid bodies with five degrees of freedom. The O–C distance was fixed to 1.16 Å, and the linearity of CO_2 was fixed with a bond angle of 180° for O–C–O. The occupancies of the C and O atoms were constrained to 2:1 because of different site multiplicities. Eventually, the analyses implied that the adsorbed CO_2 was positioned in $|Na_{12}|$-A as 24m for the carbon atoms and 48n for the oxygen atoms (Figure 7d). Therefore, one can tentatively conclude that the physisorption of CO_2 includes a bridging of Na^+ at six- and four-ring sites with the average $Na^+\cdots O{=}C{=}O\cdots Na^+$ distances of 2.70(2) and 2.72(4) Å (Table S19). These general positions were observed to be maintained also for the other compositions of zeolite A (Tables S12–S18). Bae et al.[66] have reported similar CO_2 coordination between cations on neighboring six rings on zeolite $|Na_{3.4}Ca_{4.3}|$-A.

Two remaining minor electron density peaks near the Na^+ position 12j at the four-ring sites and placed off-site of the eight-ring plane, denoted by the 24m Wyckoff coordinates,

DOI: 10.1021/acs.jpcc.8b03899
J. Phys. Chem. C 2018, 122, 17211–17220

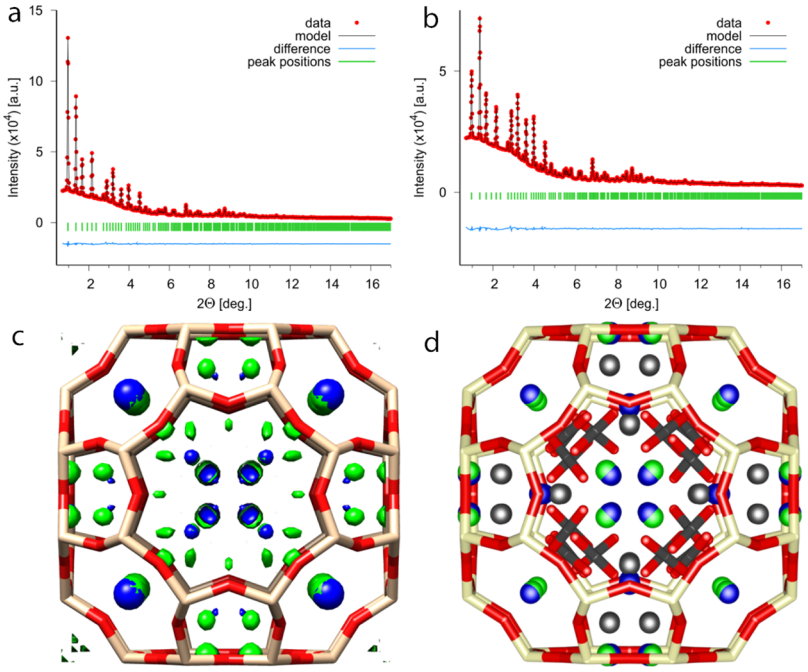

Figure 7. Rietveld refinements of (a) $|Na_{12}|$-A activated at 573 K and (b) loaded with 105 kPa CO_2. (c) Fourier maps comparing nonframework electron densities of the activated (blue) and CO_2-loaded (lime) samples. (d) Representation of the cation positions [before CO_2 loading (blue) and after (lime)] and the positions of the physisorbed (red-black sticks) and chemisorbed (black spheres) CO_2 (some low-occupied four-ring positions were removed to clarify the picture).

were tentatively attributed to chemisorbed CO_2 (Figure 7d). We modeled these sites with a single C atom, adjusting the occupancy according to the total number of electrons in CO_2 (Table S12). The apparent ratio of chemisorbed to physisorbed CO_2 for $|Na_{12}|$-A was 37:63. Because this ratio is more skewed toward chemisorption than the one reported by Cheung et al.,[41] it is highly likely that a significant amount of these positions assigned to chemisorption actually was entrapped physisorbed CO_2.

CO_2 is expected to rattle over the cavity and fill it up at relatively low pressures, but because of the high *efgs* close to the cations, it is likely strongly condensed close to the cations at low and intermediate loading levels.[23] The CO_2 molecules situated at the eight rings had been already observed for Ca-A,[66] Mg-A,[66] and chabazites.[75]

Despite the attempts to remove all structural water from the studied zeolites, signatures of residual water were observed in the α-cavity when analyzing the data for all the investigated compositions of $|Na_{12-x}K_x|$-A before and after the adsorption of CO_2 in the Fourier mappings. H_2O molecules were detected by small electron density peaks on the threefold axis, coordinated to the four-ring cations positioned inside of the main cavity. Furthermore, the overpopulated eight-ring position of $|Na_{12}|$-A was also partly assigned to adsorbed H_2O off-site of the eight-ring mirror plane. The positions of the detected H_2O followed those determined by Fischer et al.[76] for fully hydrated $|Na_{12}|$-A. The H_2O residues potentially hamper the adsorption of CO_2 to a certain extent because of the high affinity of H_2O to the adsorption sites and the hydrophilic nature of zeolite A.[77,78]

Small gas molecules are contained in the α-cavities of $|Na_{12-x}K_x|$-A and can penetrate the structure by bypassing the cations positioned in the eight rings. The gas diffusion is obstructed by the eight-ring cations and further restrained by the six-ring cations, especially when these sites are shifted into the main cavity. Because K^+ sits near the center of the eight rings and off-site of the six-ring sites, it is expected that K^+ will disturb the diffusion of gas molecules throughout $|Na_{12-x}K_x|$-A. Our earlier studies[23,42] have indicated that N_2 and CH_4 molecules are effectively blocked by K^+ at the eight-ring sites at a critical K^+ concentration, whereas CO_2 still diffuses throughout the framework structure. The adsorption of CO_2 appears to depend on the K^+ and Na^+ distributions over the six-ring and eight-ring sites.

During the in situ PXRD experiments, only the $|Na_{12}|$-A sample captured the expected amount of CO_2 (Figure 8). $|Na_{12}|$-A is known for its rapid uptake of CO_2.[40] The equilibrium adsorption levels of CO_2 on the $|Na_{12-x}K_x|$-A compositions with $x > 3$ were not achieved, as could be determined by comparing the adsorption levels from the

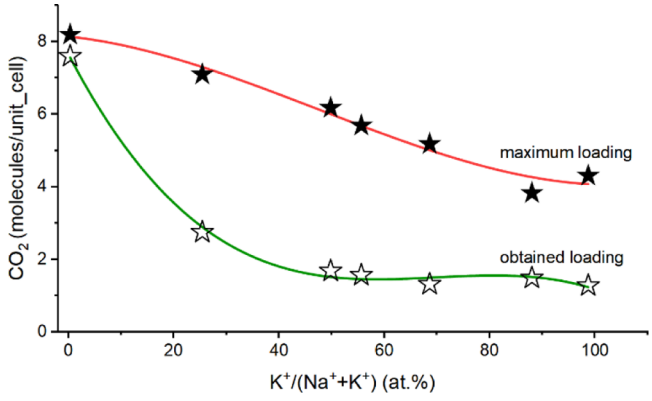

Figure 8. Number of CO_2 molecules adsorbed in the $Pm\bar{3}m$ pseudocell during the in situ XRD experiment against the maximum (equilibrated) possible loading at 105 kPa of CO_2. The lines are only guides for the eyes.

DOI: 10.1021/acs.jpcc.8b03899
J. Phys. Chem. C 2018, 122, 17211−17220

Rietveld refinements and the experimental volumetric CO_2 adsorption data. The difference between the obtained and maximum loading of CO_2 on the $|Na_{12-x}K_x|$-A is presented in Figure 8.

A detailed analysis of the PXRD data of the $|Na_{12-x}K_x|$-A samples before and after the adsorption of CO_2 revealed that the Na^+ and K^+ ions in the six and eight rings were displaced. The CO_2 molecules were adsorbed only in the α-cavities. The cation displacements on the adsorption of CO_2 are illustrated in Figure 9 and were most significant for $|Na_{12}|$-A and

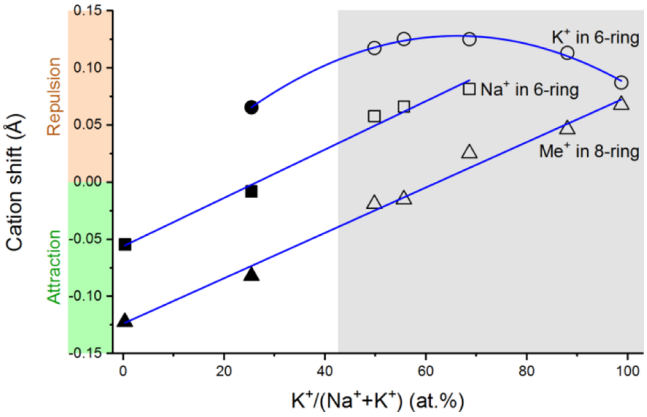

Figure 9. Shifts of extra-framework cations (Me^+) in the eight rings and Na^+ and K^+ in the six rings caused by the adsorption of CO_2, with respect to the unit cell. Blue lines are guides for the eyes. Adsorbed CO_2 attracts the extra-framework cations of $|Na_{12-x}K_x|$-A when x is small, which reduces the free space in the α-cavity (the CO_2 loading for the samples with high K^+ content was too low to study the potential repulsion in detail, gray zone).

$|Na_9K_3|$-A. However, the significance of the observations for samples with high K^+ content is hampered because of the low adsorption of CO_2 (cf. Figure 8). Na^+ in the six rings and the Na^+ or K^+ positions in the eight rings appeared to have been attracted by the CO_2 molecules for Na^+-rich compositions and experienced repulsion for K^+-rich compositions. Although K^+ in the six rings always appeared to have been repulsed by CO_2, these findings indicate that the adsorption of CO_2 contracts the cation distribution toward the center of the cavity for $|Na_{12-x}K_x|$-A when the K^+ content is low. Still, we do not want to further speculate about possible structure expansion for K^+-rich compositions.

The potential hypothesis of a redistribution of the cations across the sites upon the adsorption of CO_2 could be ruled out as the positions were occupied by the same cations before and after the adsorption of CO_2. Cation redistribution has been reported for K^+ in zeolite Rho from a window to a cage site on the adsorption of CO_2 and rationalized as a cation-gating phenomenon[26] and also observed for zeolite X on the adsorption of H_2O.[79,80] The "molecular trapdoor" mechanism has also been described for chabasite zeolites.[24,25,62,81]

CONCLUSIONS

$|Na_{12}|$-A is a promising zeolite for the removal of CO_2 from gas mixtures, and its CO_2 selectivity can be improved by a Na^+-to-K^+ ion exchange. In parallel with earlier studies, we observed that the larger K^+ ions fully replaced Na^+ in the eight-ring sites already at low K^+ content and consequently nulled the adsorption of N_2 or CH_4. In contrast to an earlier study of ours, we observed a gradual decline of the CO_2 adsorption capacity on an increasing K^+ content. K^+ gradually substituted the positions coordinated with the six rings as a function of K^+ exchange, which appeared to lower the uptake capacity of CO_2. The CO_2 over N_2 and CO_2 over CH_4 selectivities were very high for $|Na_9K_3|$-A with an $\alpha(CO_2/N_2)$ >21 000 and $\alpha(CO_2/CH_4)$ >8000 as compared to the corresponding $\alpha(CO_2/N_2)$ ~800 and $\alpha(CO_2/CH_4)$ ~400 for $|Na_{12}|$-A.

The in situ PXRD experiments were used to reveal the structural alternations of $|Na_{12-x}K_x|$-A at an atomic resolution on the adsorption of CO_2. However, only the $|Na_{12}|$-A sample appeared to have demonstrated a sufficiently rapid uptake of CO_2 during the experiments. For the other compositions, the Rietveld analysis showed less adsorbed CO_2 molecules as compared with those determined by volumetric adsorption experiments. The observed decreases of the intensities of certain Bragg peaks after the adsorption of CO_2 in $|Na_{12-x}K_x|$-A were related to the displacement of K^+ and Na^+. Adsorbed CO_2 molecules were determined to bridge cations at the six- and four-ring sites and to be involved in the displacement of the related Na^+ and K^+. In addition, adsorbed CO_2 molecules appeared to be strongly coordinated by cations at the four- and eight-ring sites of $|Na_{12}|$-A. From the analysis of the in situ PXRD data, we concluded that CO_2 had imposed an attraction on the cations at the six- and eight-ring sites in the Na^+-rich samples. An indication of a repulsion of the extra-framework positions by the CO_2 molecules was observed for the K^+-rich samples, but as those samples were not fully equilibrated during the PXRD experiments, the conclusions remain uncertain. Further investigations by using, for example, in situ neutron powder diffraction could be warranted to quantify the positional changes of Na^+ and K^+ in $|Na_{12-x}K_x|$-A and specifically the positions for adsorbed CO_2. Neutrons are more sensitive for C (b = 6.65 fm) and O (b = 5.81 fm) than X-rays.

ASSOCIATED CONTENT

Supporting Information

The Supporting Information is available free of charge on the ACS Publications website at DOI: 10.1021/acs.jpcc.8b03899.

Ion-exchange procedure; parameters for the adsorption models (dual-site Langmuir and Henry's law) for the adsorption of CO_2, N_2, and CH_4 on $|Na_{12}|$-A and $|Na_9K_3|$-A; atomic positions, occupancies, and displacements for all samples; selected interatomic distances and angles; Rietveld analysis data for all samples; and Fourier maps of extra-framework cations and CO_2 for all samples (PDF)

AUTHOR INFORMATION

Corresponding Authors

*E-mail: wardecki@chalmers.se (D.W.).
*E-mail: niklas.hedin@mmk.su.se (N.H.).

ORCID

Stef Smeets: 0000-0002-5413-9038
Xiaodong Zou: 0000-0001-6748-6656
Niklas Hedin: 0000-0002-7284-2974

Notes

The authors declare the following competing financial interest(s): N.H. is a cofounder and co-owner of SIA NeoZeo commercializing adsorption-driven biogas upgrading.

DOI: 10.1021/acs.jpcc.8b03899
J. Phys. Chem. C 2018, 122, 17211−17220

■ ACKNOWLEDGMENTS

This research was financially supported by the Swedish Energy Agency, the Swedish Research Council (VR), the Swedish Governmental Agency for Innovation Systems (VINNOVA) through the Berzelii Center EXSELENT. The Innovation Fund Denmark and the HiGradeGas project (grant no. 5157-00008B) are acknowledged. We also acknowledge the support from MATsynCELL project through the Röntgen−Ångström Cluster. We would like to thank PETRA-III at DESY Deutsches Elektronen-Synchrotron for the possibility of running the in situ experiment at the high-resolution PXRD beamline and Dr. Martin Etter for his help with setting up the experiment. S.S. thanks the Swiss National Science Foundation for financial support (project number: 177761).

■ REFERENCES

(1) Moss, R. H.; Edmonds, J. A.; Hibbard, K. A.; Manning, M. R.; Rose, S. K.; van Vuuren, D. P.; Carter, T. R.; Emori, S.; Kainuma, M.; Meehl, G. A.; et al. The next Generation of Scenarios for Climate Change Research and Assessment. *Nature* **2010**, *463*, 747−756.

(2) Root, T. L.; Price, J. T.; Hall, K. R.; Schneider, S. H.; Rosenzweig, C.; Pounds, J. A. Fingerprints of Global Warming on Wild Animals and Plants. *Nature* **2003**, *421*, 57−60.

(3) Haszeldine, R. S. Carbon Capture and Storage: How Green Can Black Be? *Science* **2009**, *325*, 1647−1652.

(4) Leung, D. Y. C.; Caramanna, G.; Maroto-Valer, M. M. An Overview of Current Status of Carbon Dioxide Capture and Storage Technologies. *Renewable Sustainable Energy Rev.* **2014**, *39*, 426−443.

(5) Choi, S.; Drese, J. H.; Jones, C. W. Adsorbent Materials for Carbon Dioxide Capture from Large Anthropogenic Point Sources. *ChemSusChem* **2009**, *2*, 796−854.

(6) Hasan, M. M. F.; First, E. L.; Floudas, C. A. Cost-effective CO_2 capture based on in silico screening of zeolites and process optimization. *Phys. Chem. Chem. Phys.* **2013**, *15*, 17601−17618.

(7) Webley, P. A. Adsorption technology for CO_2 separation and capture: a perspective. *Adsorption* **2014**, *20*, 225−231.

(8) Boot-Handford, M. E.; Abanades, J. C.; Anthony, E. J.; Blunt, M. J.; Brandani, S.; Mac Dowell, N.; Fernández, J. R.; Ferrari, M.-C.; Gross, R.; Hallett, J. P.; et al. Carbon Capture and Storage Update. *Energy Environ. Sci.* **2014**, *7*, 130−189.

(9) Wang, D.; Zhao, T.; Cao, Y.; Yao, S.; Li, G.; Huo, Q.; Liu, Y. High performance gas adsorption and separation of natural gas in two microporous metal-organic frameworks with ternary building units. *Chem. Commun.* **2014**, *50*, 8648−8650.

(10) Duan, J.; Jin, W.; Krishna, R. Natural Gas Purification Using a Porous Coordination Polymer with Water and Chemical Stability. *Inorg. Chem.* **2015**, *54*, 4279−4284.

(11) Sun, Q.; Li, H.; Yan, J.; Liu, L.; Yu, Z.; Yu, X. Selection of Appropriate Biogas Upgrading Technology-a Review of Biogas Cleaning, Upgrading and Utilisation. *Renewable Sustainable Energy Rev.* **2015**, *51*, 521−532.

(12) Edwards, R.; Hass, H.; Larivé, J.-F.; Lonza, L.; Mass, H.; Rickeard, D.; Larive, J.-F.; Rickeard, D.; Weindorf, W. *Well-to-Wheels Analysis of Future Automotive Fuels and Powertrains in the European Context WELL-TO-TANK (WTT) Report* Version 4; 2014.

(13) Moliner, M.; Martínez, C.; Corma, A. Synthesis Strategies for Preparing Useful Small Pore Zeolites and Zeotypes for Gas Separations and Catalysis. *Chem. Mater.* **2014**, *26*, 246−258.

(14) Olaizola, M. Microalgal removal of CO_2 from flue gases: Changes in medium pH and flue gas composition do not appear to affect the photochemical yield of microalgal cultures. *Biotechnol. Bioprocess Eng.* **2003**, *8*, 360−367.

(15) Kang, S.-P.; Lee, H. Recovery of CO_2 from Flue Gas Using Gas Hydrate: Thermodynamic Verification through Phase Equilibrium Measurements. *Environ. Sci. Technol.* **2000**, *34*, 4397−4400.

(16) Satyapal, S.; Filburn, T.; Trela, J.; Strange, J. Performance and Properties of a Solid Amine Sorbent for Carbon Dioxide Removal in Space Life Support Applications. *Energy Fuels* **2001**, *15*, 250−255.

(17) Weast, R.; Astle, M.; Beyer, W. *CRC Handbook of Chemistry and Physics*; CRC Press, 1989.

(18) Cheung, O.; Hedin, N. Zeolites and related sorbents with narrow pores for CO_2 separation from flue gas. *RSC Adv.* **2014**, *4*, 14480−14494.

(19) Breck, D. W. Zeolite Molecular Sieves: Structure, Chemistry, and Use. *J. Chromatogr. Sci.* **1975**, *13*, 18A.

(20) D'Alessandro, D. M.; Smit, B.; Long, J. R. Carbon Dioxide Capture: Prospects for New Materials. *Angew. Chem., Int. Ed.* **2010**, *49*, 6058−6082.

(21) Zhang, J.; Singh, R.; Webley, P. A. Alkali and alkaline-earth cation exchanged chabazite zeolites for adsorption based CO2 capture. *Microporous Mesoporous Mater.* **2008**, *111*, 478−487.

(22) Ridha, F. N.; Yang, Y.; Webley, P. A. Adsorption Characteristics of a Fully Exchanged Potassium Chabazite Zeolite Prepared from Decomposition of Zeolite Y. *Microporous Mesoporous Mater.* **2009**, *117*, 497−507.

(23) Liu, Q.; Mace, A.; Bacsik, Z.; Sun, J.; Laaksonen, A.; Hedin, N. NaKA sorbents with high CO_2-over-N_2 selectivity and high capacity to adsorb CO_2. *Chem. Commun.* **2010**, *46*, 4502−4504.

(24) Shang, J.; Li, G.; Singh, R.; Xiao, P.; Liu, J. Z.; Webley, P. A. Determination of Composition Range for "Molecular Trapdoor" Effect in Chabazite Zeolite. *J. Phys. Chem. C* **2013**, *117*, 12841−12847.

(25) Shang, J.; Li, G.; Singh, R.; Gu, Q.; Nairn, K. M.; Bastow, T. J.; Medhekar, N.; Doherty, C. M.; Hill, A. J.; Liu, J. Z.; et al. Discriminative Separation of Gases by a "Molecular Trapdoor" Mechanism in Chabazite Zeolites. *J. Am. Chem. Soc.* **2012**, *134*, 19246−19253.

(26) Lozinska, M. M.; Mowat, J. P. S.; Wright, P. A.; Thompson, S. P.; Jorda, J. L.; Palomino, M.; Valencia, S.; Rey, F. Cation Gating and Relocation during the Highly Selective "Trapdoor" Adsorption of CO_2 on Univalent Cation Forms of Zeolite Rho. *Chem. Mater.* **2014**, *26*, 2052−2061.

(27) Lozinska, M. M.; Mangano, E.; Mowat, J. P. S.; Shepherd, A. M.; Howe, R. F.; Thompson, S. P.; Parker, J. E.; Brandani, S.; Wright, P. A. Understanding Carbon Dioxide Adsorption on Univalent Cation Forms of the Flexible Zeolite Rho at Conditions Relevant to Carbon Capture from Flue Gases. *J. Am. Chem. Soc.* **2012**, *134*, 17628−17642.

(28) García, E. J.; Mowat, J. P. S.; Wright, P. A.; Pérez-Pellitero, J.; Jallut, C.; Pirngruber, G. D. Role of Structure and Chemistry in Controlling Separations of CO_2/CH_4 and $CO_2/CH_4/CO$ Mixtures over Honeycomb MOFs with Coordinatively Unsaturated Metal Sites. *J. Phys. Chem. C* **2012**, *116*, 26636−26648.

(29) Coudert, F.-X.; Kohen, D. Molecular Insight into CO_2 "Trapdoor" Adsorption in Zeolite Na-RHO. *Chem. Mater.* **2017**, *29*, 2724−2730.

(30) Lozinska, M. M.; Mangano, E.; Greenaway, A. G.; Fletcher, R.; Thompson, S. P.; Murray, C. A.; Brandani, S.; Wright, P. A. Cation Control of Molecular Sieving by Flexible Li-Containing Zeolite Rho. *J. Phys. Chem. C* **2016**, *120*, 19652−19662.

(31) Pham, T. D.; Hudson, M. R.; Brown, C. M.; Lobo, R. F. On the Structure-Property Relationships of Cation-Exchanged ZK-5 Zeolites for CO_2 Adsorption. *ChemSusChem* **2017**, *10*, 946−957.

(32) Breck, D. W.; Eversole, W. G.; Milton, R. M.; Reed, T. B.; Thomas, T. L. Crystalline Zeolites. I. The Properties of a New Synthetic Zeolite, Type A. *J. Am. Chem. Soc.* **1956**, *78*, 5963−5972.

(33) Reed, T. B.; Breck, D. W. Crystalline Zeolites. II. Crystal Structure of Synthetic Zeolite, Type A. *J. Am. Chem. Soc.* **1956**, *78*, 5972−5977.

(34) Hayashi, H.; Côté, A. P.; Furukawa, H.; O'Keeffe, M.; Yaghi, O. M. Zeolite A Imidazolate Frameworks. *Nat. Mater.* **2007**, *6*, 501−506.

(35) Grämlich, V.; Meier, W. M. The crystal structure of hydrated NaA: A detailed refinement of a pseudosymmetric zeolite structure*. *Z. Kristallogr. - New Cryst. Struct.* **1971**, *133*, 134−149.

DOI: 10.1021/acs.jpcc.8b03899
J. Phys. Chem. C 2018, 122, 17211−17220

(36) Kim, H.; Cho, H. S.; Kim, C.; Choi, M. Gradual Disordering of LTA Zeolite for Continuous Tuning of the Molecular Sieving Effect. *J. Phys. Chem. C* **2017**, *121*, 6807−6812.
(37) Hedin, N.; DeMartin, G. J.; Strohmaier, K. G.; Reyes, S. C. PFG NMR Self-Diffusion of Propylene in ITQ-29, CaA and NaCaA: Window Size and Cation Effects. *Microporous Mesoporous Mater.* **2007**, *98*, 182−188.
(38) Price, L.; Leung, K.; Sartbaeva, A. Local and Average Structural Changes in Zeolite A upon Ion Exchange. *Magnetochemistry* **2017**, *3*, 42.
(39) Sun, H.; Wu, D.; Liu, K.; Guo, X.; Navrotsky, A. Energetics of Alkali and Alkaline Earth Ion-Exchanged Zeolite A. *J. Phys. Chem. C* **2016**, *120*, 15251−15256.
(40) Cheung, O.; Bacsik, Z.; Liu, Q.; Mace, A.; Hedin, N. Adsorption kinetics for CO_2 on highly selective zeolites NaKA and nano-NaKA. *Appl. Energy* **2013**, *112*, 1326−1336.
(41) Cheung, O.; Bacsik, Z.; Krokidas, P.; Mace, A.; Laaksonen, A.; Hedin, N.; et al. K^+ Exchanged Zeolite ZK-4 as a Highly Selective Sorbent for CO_2. *Langmuir* **2014**, *30*, 9682−9690.
(42) Cheung, O.; Wardecki, D.; Bacsik, Z.; Vasiliev, P.; McCusker, L. B.; Hedin, N. Highly selective uptake of carbon dioxide on the zeolite $|Na_{10.2}KCs_{0.8}|$-LTA—a possible sorbent for biogas upgrading. *Phys. Chem. Chem. Phys.* **2016**, *18*, 16080−16083.
(43) Bacsik, Z.; Cheung, O.; Vasiliev, P.; Hedin, N. Selective separation of CO_2 and CH_4 for biogas upgrading on zeolite NaKA and SAPO-56. *Appl. Energy* **2016**, *162*, 613−621.
(44) Bulow, M.; Guo, C. J.; Shen, D.; Fitch, F. R.; Shirley, A. I.; La Cava, A. I.; Dougill, S. B.; Brooks, J. P. Separation of Carbon Dioxide and Hydrocarbons. U.S. Patent 6,024,781A 2000.
(45) Fang, H.; Kulkarni, A.; Kamakoti, P.; Awati, R.; Ravikovitch, P. I.; Sholl, D. S. Identification of High-CO_2-Capacity Cationic Zeolites by Accurate Computational Screening. *Chem. Mater.* **2016**, *28*, 3887−3896.
(46) Ojuva, A.; Järveläinen, M.; Bauer, M.; Keskinen, L.; Valkonen, M.; Akhtar, F.; Levänen, E.; Bergström, L. Mechanical performance and CO_2 uptake of ion-exchanged zeolite A structured by freeze-casting. *J. Eur. Ceram. Soc.* **2015**, *35*, 2607−2618.
(47) Thakkar, H.; Eastman, S.; Hajari, A.; Rownaghi, A. A.; Knox, J. C.; Rezaei, F. 3D-Printed Zeolite Monoliths for CO_2 Removal from Enclosed Environments. *ACS Appl. Mater. Interfaces* **2016**, *8*, 27753−27761.
(48) Palomino, M.; Corma, A.; Rey, F.; Valencia, S. New Insights on CO_2−Methane Separation Using LTA Zeolites with Different Si/Al Ratios and a First Comparison with MOFs. *Langmuir* **2010**, *26*, 1910−1917.
(49) Akhtar, F.; Liu, Q.; Hedin, N.; Bergström, L. Strong and binder free structured zeolite sorbents with very high CO_2-over-N_2 selectivities and high capacities to adsorb CO_2 rapidly. *Energy Environ. Sci.* **2012**, *5*, 7664.
(50) Pluth, J. J.; Smith, J. V. Accurate redetermination of crystal structure of dehydrated zeolite A. Absence of near zero coordination of sodium. Refinement of silicon, aluminum-ordered superstructure. *J. Am. Chem. Soc.* **1980**, *102*, 4704−4708.
(51) Pluth, J. J.; Smith, J. V. Crystal Structure of Dehydrated Potassium-Exchanged Zeolite A. Absence of Supposed Zero-Coordinated Potassium. Refinement of Silicon, Aluminum-Ordered Superstructure. *J. Phys. Chem.* **1979**, *83*, 741−749.
(52) Leung, P. C. W.; Kunz, K. B.; Seff, K.; Maxwell, I. E. Crystal Structures of Hydrated and Dehydrated Potassium-Exchanged Zeolite A. *J. Phys. Chem.* **1975**, *79*, 2157−2162.
(53) Subramanian, V.; Seff, K. A near Zero Coordinate Sodium Ion in Dehydrated Zeolite 4A, Na_{12}-A. *J. Phys. Chem.* **1977**, *81*, 2249−2251.
(54) Yoshida, K.; Toyoura, K.; Matsunaga, K.; Nakahira, A.; Kurata, H.; Ikuhara, Y. H.; Sasaki, Y. Structural Analyses of Sodium Cations Embedded within Zeolitic Nanocavities. *Microporous Mesoporous Mater.* **2018**, *259*, 195−202.
(55) Guo, X.; Wu, L.; Navrotsky, A. Thermodynamic evidence of flexibility in H_2O and CO_2 absorption of transition metal ion exchanged zeolite LTA. *Phys. Chem. Chem. Phys.* **2018**, *20*, 3970−3978.
(56) Finkelstein, Y.; Saig, A.; Danon, A.; Koresh, J. E. Study of Type-A Zeolites. Part 1: Mechanism of He and Ne Encapsulation. *J. Phys. Chem. B* **2003**, *107*, 9170−9174.
(57) Hammersley, A. P. *FIT2D: An Introduction and Overview*. European Synchrotron Radiation. Facilty International Report ESRF97HA02T 1997; Vol *68*, p 58.
(58) Coelho, A. A. TOPAS and TOPAS-Academic: an optimization program integrating computer algebra and crystallographic objects written in C++. *J. Appl. Crystallogr.* **2018**, *51*, 210−218.
(59) Coelho, A. A. *Topas-Academic*; Coelho Software: Brisbane, Australia 2007.
(60) Delaval, Y.; de Lara, E. C. Study of physisorption of carbon dioxide on naa zeolite. Part 1.-Experimental results obtained by infrared spectroscopy. *J. Chem. Soc., Faraday Trans. 1* **1981**, *77*, 869−877.
(61) Delaval, Y.; Seloudoux, R.; de Lara, E. C. Determination of isotherms and initial heat of adsorption of CO_2 and N_2O in four A zeolites from infrared measurements. *J. Chem. Soc. Faraday Trans. 1* **1986**, *82*, 365.
(62) De Baerdemaeker, T.; De Vos, D. Trapdoors in zeolites. *Nat. Chem.* **2013**, *5*, 89−90.
(63) Siriwardane, R. V.; Shen, M.-S.; Fisher, E. P.; Losch, J. Adsorption of CO_2 on Zeolites at Moderate Temperatures. *Energy Fuels* **2005**, *19*, 1153−1159.
(64) Förster, H.; Schumann, M. Infrared spectroscopic studies on carbon dioxide adsorption in alkali-metal and alkaline-earth-metal ion-exchanged A-type zeolites. Part 1.-General features of CO_2 interaction with A-type zeolites. *J. Chem. Soc., Faraday Trans. 1* **1989**, *85*, 1149.
(65) Amari, D.; Cuesta, J. M. L.; Nguyen, N. P.; Jerrentrup, R.; Ginoux, J. L. Chemisorption and physisorption of CO_2 on cation exchanged zeolitesA, X and mor. *J. Therm. Anal.* **1992**, *38*, 1005−1015.
(66) Bae, T.-H.; Hudson, M. R.; Mason, J. A.; Queen, W. L.; Dutton, J. J.; Sumida, K.; Micklash, K. J.; Kaye, S. S.; Brown, C. M.; Long, J. R. Evaluation of Cation-Exchanged Zeolite Adsorbents for Post-Combustion Carbon Dioxide Capture. *Energy Environ. Sci.* **2013**, *6*, 128−138.
(67) Mathias, P. M.; Kumar, R.; Moyer, J. D.; Schork, J. M.; Srinivasan, S. R.; Auvil, S. R.; Talu, O. Correlation of Multicomponent Gas Adsorption by the Dual-Site Langmuir Model. Application to Nitrogen/Oxygen Adsorption on 5A-Zeolite. *Ind. Eng. Chem. Res.* **1996**, *35*, 2477−2483.
(68) Ridha, F. N.; Webley, P. A. Anomalous Henry's law behavior of nitrogen and carbon dioxide adsorption on alkali-exchanged chabazite zeolites. *Sep. Purif. Technol.* **2009**, *67*, 336−343.
(69) Maurer, S.; Mersmann, A.; Peukert, W. Henry Coefficients of Adsorption Predicted from Solid Hamaker Constants. *Chem. Eng. Sci.* **2001**, *56*, 3443−3453.
(70) Li, P.; Handan Tezel, F. Adsorption separation of N_2, O_2, CO_2 and CH_4 gases by β-zeolite. *Microporous Mesoporous Mater.* **2007**, *98*, 94−101.
(71) Akten, E. D.; Siriwardane, R.; Sholl, D. S. Monte Carlo Simulation of Single- and Binary-Component Adsorption of CO_2, N_2, and H_2 in Zeolite Na-4A. *Energy Fuels* **2003**, *17*, 977−983.
(72) Ghoufi, A.; Gaberova, L.; Rouquerol, J.; Vincent, D.; Llewellyn, P. L.; Maurin, G. Adsorption of CO_2, CH_4 and their binary mixture in Faujasite NaY: A combination of molecular simulations with gravimetry-manometry and microcalorimetry measurements. *Microporous Mesoporous Mater.* **2009**, *119*, 117−128.
(73) Koller, H.; Meijer, E. L.; van Santen, R. A. ^{27}Al quadrupole interaction in zeolites loaded with probe molecules-a quantum-chemical study of trends in electric field gradients and chemical bonds in clusters. *Solid State Nucl. Magn. Reson.* **1997**, *9*, 165−175.
(74) Graham, C.; Imrie, D. A.; Raab, R. E. Measurement of the electric quadrupole moments of CO_2, CO, N_2, Cl_2 and BF_3. *Mol. Phys.* **1998**, *93*, 49−56.

DOI: 10.1021/acs.jpcc.8b03899
J. Phys. Chem. C 2018, 122, 17211−17220

(75) Hudson, M. R.; Queen, W. L.; Mason, J. A.; Fickel, D. W.; Lobo, R. F.; Brown, C. M. Unconventional, Highly Selective CO2 Adsorption in Zeolite SSZ-13. *J. Am. Chem. Soc.* **2012**, *134*, 1970−1973.
(76) Fischer, R. X.; Sehovic, M.; Baur, W. H.; Paulmann, C.; Gesing, T. M. Crystal Structure and Morphology of Fully Hydrated Zeolite Na-A. *Z. Kristallogr.* **2012**, *227*, 438−445.
(77) McDonnell, A. M. P.; Beving, D.; Wang, A.; Chen, W.; Yan, Y. Hydrophilic and Antimicrobial Zeolite Coatings for Gravity-Independent Water Separation. *Adv. Funct. Mater.* **2005**, *15*, 336−340.
(78) Castillo, J. M.; Silvestre-Albero, J.; Rodriguez-Reinoso, F.; Vlugt, T. J. H.; Calero, S. Water Adsorption in Hydrophilic Zeolites: Experiment and Simulation. *Phys. Chem. Chem. Phys.* **2013**, *15*, 17374.
(79) Jeffroy, M.; Borissenko, E.; Boutin, A.; Di Lella, A.; Porcher, F.; Souhassou, M.; Lecomte, C.; Fuchs, A. H. Evidence of a Framework Induced Cation Redistribution upon Water Adsorption in Cobalt Exchanged X Faujasite Zeolite: A Joint Experimental and Simulation Study. *Microporous Mesoporous Mater.* **2011**, *138*, 45−50.
(80) Beauvais, C.; Boutin, A.; Fuchs, A. H. A Numerical Evidence for Nonframework Cation Redistribution upon Water Adsorption in Faujasite Zeolite. *ChemPhysChem* **2004**, *5*, 1791−1793.
(81) Shang, J.; Li, G.; Gu, Q.; Singh, R.; Xiao, P.; Liu, J. Z.; Webley, P. A. Temperature controlled invertible selectivity for adsorption of N_2 and CH_4 by molecular trapdoor chabazites. *Chem. Commun.* **2014**, *50*, 4544−4546.

DOI: 10.1021/acs.jpcc.8b03899
J. Phys. Chem. C 2018, 122, 17211−17220